MATHEMATICAL BIOSCIENCES
AND ENGINEERING
Volume **2**, Number **3**, August **2005**

http://www.mbejournal.org/

pp. **445–460**

INTERSTITIAL PRESSURE AND EXTRACELLULAR FLUID MOTION IN TUMOR CORDS

Alessandro Bertuzzi

Istituto di Analisi dei Sistemi ed Informatica "A. Ruberti", CNR
Viale Manzoni 30, 00185 Roma, Italy

Antonio Fasano

Dipartimento di Matematica "U. Dini", Università di Firenze
Viale Morgagni 67/A, 50134 Firenze, Italy

Alberto Gandolfi

Istituto di Analisi dei Sistemi ed Informatica "A. Ruberti", CNR
Viale Manzoni 30, 00185 Roma, Italy

Carmela Sinisgalli

Istituto di Analisi dei Sistemi ed Informatica "A. Ruberti", CNR
Viale Manzoni 30, 00185 Roma, Italy

Abstract. This work illustrates the behavior of the interstitial pressure and of the interstitial fluid motion in tumor cords (cylindrical arrangements of tumor cells growing around blood vessels of the tumor) by means of numerical simulations on the basis of a mathematical model previously developed. The model describes the steady state of a tumor cord surrounded by necrosis and its time evolution following cell killing. The most relevant aspects of the dynamics of extracellular fluid are by computing the longitudinal average of the radial fluid velocity and of the pressure field. In the present paper, the necrotic region is treated as a mixture of degrading dead cells and fluid.

1. **Introduction.** Blood flow in the tumor vasculature plays a crucial role in tumor growth and in the therapy. Blood carries oxygen and nutrients necessary for cell viability and proliferation and allows drugs or other therapeutic agents to be delivered inside the tumor. To reach their target cells, these agents must extravasate and be transported by diffusion and by the convection caused by the motion of extracellular fluid. Convective transport becomes important in the case of novel therapeutic agents characterized by large molecular weight or size, such as the monoclonal antibodies or the viral particles used as vectors in gene therapy [13]. It is known that most solid tumors exhibit high interstitial fluid pressure. In a set of ten experimental and human tumors, pressure values ranging from 4.5 to 38 mmHg have been reported, the majority of these values (7 out of 10) being between 10 and 23 mmHg [13]. The high interstitial pressure is thought to be a barrier for fluid extravasation and for an efficient convective transport. Mathematical models that describe the interstitial pressure field and the macroscopic fluid flow in spherical

2000 *Mathematics Subject Classification.* 35R35, 92C37, 92C50.

Key words and phrases. tumor growth, interstitial pressure, extracellular fluid, cancer treatment, PDE modeling, free boundary problems.

tumors have been proposed in [4, 20], assuming a continuous distribution of fluid sources in the tumor mass. The localized discrete nature of the fluid sources has been taken into account in [3], where a pair of countercurrent vessels and an ideal two-dimensional regular mesh of vessels were modelled.

In our work, extracellular fluid motion and interstitial pressure are studied in a regular array of tumor cords, each cord being surrounded by necrosis. Although the vascular network of tumors is in general highly irregular, in some human and experimental tumors it is possible to observe cylindrical arrangements of tumor cells around central blood vessels (tumor cords [19, 12, 16]). The decrease of oxygen and nutrients as the distance from the central vessel increases produces the formation of necrosis in the regions far from the vessels. A mathematical model that describes the behavior of a system of tumor cords under the influence of a therapeutic treatment was proposed in [7]. That model, based on the continuum approach, included the diffusion of oxygen from the central vessel and the cell motion and was used to predict the cord response to single-dose cytotoxic treatments [6]. The computation of the flow of interstitial fluid was avoided in [6, 7], confining the study to cases in which drug convection by the fluid is negligible. In a recent paper [8], we incorporated in the previous theory the relevant information about the flow of interstitial fluid within the tumor cord and the associated pressure field. Moreover, unlike [6, 7], the necrotic region was viewed simply as a chamber filled with a homogeneous fluid whose uniform pressure is related to the mechanical interaction of the tumor with the surrounding tissue. Existence and uniqueness of the stationary solution of this model was proved, together with the existence and uniqueness of the solution for the time-dependent problem.

In this paper, we summarize the model proposed in [8] (sections 2 and 3), and provide numerical solutions of model equations. Thus we can illustrate the effect of parameter changes on the behavior of interstitial pressure and interstitial fluid motion, both in the stationary state (section 4) and during the time evolution following the treatment (section 5). A new description of the necrotic region is here presented, which, in contrast with [8], accounts for the presence in that region of a mixture of degrading dead cells and fluid.

2. **The mathematical model.**

In this section we summarize, for the reader's convenience, the tumor cord model proposed in [8], and we present the new description of the necrotic region. We consider an ideal regular array of parallel and identical tumor cords inside the tumor mass, as in the Krogh model of microcirculation [14], each cord being separated from others by a region of necrosis. Vessels are assumed to be displaced as the tumor mass is growing or regressing, and the treatment is assumed not to degrade the tumor vasculature. We assume cylindrical symmetry around the axis of the central blood vessel, the radial coordinate r varying between the radius r_0 of the blood vessel and the unknown outer boundary B of the necrotic region surrounding each cord. The radius of the interface between the cord and the necrosis is denoted by ρ_N. Because of the radial symmetry of the system of cords, no exchange of matter occurs through the boundary $r = B$. The axial coordinate z will range in the interval $[-H, H]$ (see Fig. 1). All the quantities involved depend at most on r, z, and the time t. Only one species of nutrient is considered, as in previous models of tumor growth (see [10, 5, 2, 11]), and we identify this critical nutrient with oxygen. We do not distinguish the intracellular from the extracellular concentration of oxygen, and we denote by σ its local concentration.

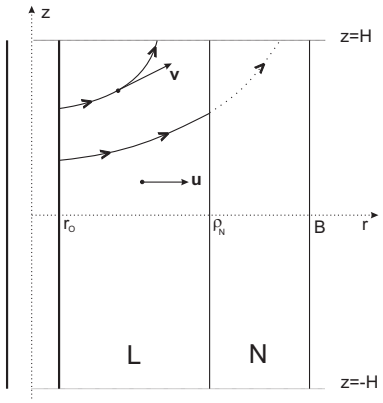

FIGURE 1. Scheme of the tumor cord geometry: L, tumor cord; N, necrotic region. The vector **u** indicates the cellular velocity; the vector **v** indicates the extracellular fluid velocity.

2.1. **Cell populations, oxygen diffusion, and cord radius.** Three components are present in the cord:

1. The viable cells, which are subdivided into proliferating cells (P) and quiescent cells (Q) in view of their possibly different sensitivity to treatment. Cell decycling into quiescence and cell recruitment from quiescence into proliferation are assumed to be regulated by the oxygen concentration, as suggested by experimental observations [1, 18] and proposed in [11].
2. The dead cells resulting from treatment, which are present in the form of apoptotic bodies (A). Unlike the approach in [6, 7], spontaneous cell death within the viable region is disregarded, since its extent appears to be small [16].
3. The extracellular fluid filling interstitial space.

Describing the system as a continuum, we introduce the fractions of volume occupied locally by these components. These fractions are denoted by ν_P, ν_Q, ν_A, and ν_E, respectively. Supposing no voids, we have

$$\nu_P + \nu_Q + \nu_A + \nu_E = 1\,.$$

As in [6, 7], it is assumed that (i) the volume fraction of extracellular fluid in the cord is constant even during treatment; (ii) dead cells move at the same velocity as living cells; (iii) the cell velocity is radial; (iv) the oxygen concentration, the volume fractions ν_P, ν_Q, ν_A, and the velocity of cellular material do not depend on the longitudinal coordinate z; (v) cells die if σ reaches a death threshold σ_N. A discussion on the above assumptions was given in [8]. For the cell velocity field **u**, we have, in view of assumptions (iii) and (iv), $\mathbf{u} = (u_r,\, u_z) = (u(r,t),\, 0)$. The velocity field of the fluid component is denoted by $\mathbf{v} = (v_r(r,z,t),\, v_z(r,z,t))$.

Making the reasonable assumption that all the components have the same mass density and are incompressible, the mass balance equations can be written as follows:

$$\frac{\partial \nu_P}{\partial t} + \nabla \cdot (\nu_P \, \mathbf{u}) = \chi \nu_P + \gamma(\sigma)\nu_Q - \lambda(\sigma)\nu_P - \mu_P(r,t)\nu_P \,, \tag{1}$$

$$\frac{\partial \nu_Q}{\partial t} + \nabla \cdot (\nu_Q \, \mathbf{u}) = -\gamma(\sigma)\nu_Q + \lambda(\sigma)\nu_P - \mu_Q(r,t)\nu_Q \,, \tag{2}$$

$$\frac{\partial \nu_A}{\partial t} + \nabla \cdot (\nu_A \, \mathbf{u}) = \alpha\big[\mu_P(r,t)\nu_P + \mu_Q(r,t)\nu_Q\big] - \mu_A \nu_A \,, \tag{3}$$

$$\nu_E \nabla \cdot \mathbf{v} = (1-\alpha)\big[\mu_P(r,t)\nu_P + \mu_Q(r,t)\nu_Q\big] + \mu_A \nu_A - \chi \nu_P \,. \tag{4}$$

In equations (1)–(4), $\chi > 0$ is the rate constant of volume increment due to cell proliferation; the functions $\gamma(\sigma)$ and $\lambda(\sigma)$ are the rates of the transitions $Q \to P$ and $P \to Q$, respectively; μ_P and μ_Q are death rates that mimic the killing effects of drugs or radiation, taken here as assigned functions of r and t; $\alpha < 1$ is the fraction of the volume of a cell dying by apoptosis, which is converted into apoptotic bodies, the fraction $1-\alpha$ going to the extracellular liquid (a loss of volume has been observed indeed during the early phase of apoptosis [15]); $\mu_A > 0$ is the rate of volume loss due to degradation of apoptotic bodies to a liquid waste. According to the experimental evidence, the function $\lambda(\sigma)$ will be nonincreasing and $\gamma(\sigma)$ nondecreasing. In particular, we assign two threshold values for σ, $\sigma_Q < \sigma_P$, and we assume $\lambda = \lambda_{max}$ and $\gamma = \gamma_{min}$ for $\sigma \le \sigma_Q$, $\lambda = \lambda_{min}$ and $\gamma = \gamma_{max}$ for $\sigma \ge \sigma_P$, with $\lambda_{max} > \lambda_{min} \ge 0$ and $\gamma_{max} > \gamma_{min} \ge 0$. In the interval (σ_Q, σ_P), $\lambda(\sigma)$ decreases linearly and $\gamma(\sigma)$ increases linearly.

By setting $\nu^\star = \nu_P + \nu_Q + \nu_A = 1 - \nu_E$, which is constant in view of assumption (i), we can derive the equation for $u(r,t)$ by summing (1)–(3). We obtain

$$\nu^\star \frac{1}{r}\frac{\partial}{\partial r}(ru) = \chi \nu_P - (1-\alpha)(\mu_P \nu_P + \mu_Q \nu_Q) - \mu_A(\nu^\star - \nu_P - \nu_Q) \,. \tag{5}$$

Equation (5) will be completed by the boundary condition

$$u(r_0, t) = 0 \,.$$

Concerning the equation for σ, diffusion is the dominant transport mechanism for oxygen, and it occurs in a quasi-stationary regime because of the high oxygen diffusivity [19] and the comparatively slow cellular dynamics. Thus we have

$$\Delta \sigma = f_P(\sigma)\nu_P + f_Q(\sigma)\nu_Q \,,$$

with the boundary conditions

$$\sigma(r_0, t) = \sigma_b \tag{6}$$

$$\left.\frac{\partial \sigma}{\partial r}\right|_{r=\rho_N(t)} = 0 \,, \tag{7}$$

where $f_P(\sigma)$, $f_Q(\sigma)$ denote the ratio between the consumption rate per unit volume of proliferating and quiescent cells, respectively, and the diffusion coefficient. We set $f_P(\sigma) \ge f_Q(\sigma)$ and require $f_Q(\sigma_N) > 0$. At the inner boundary $r = r_0$ (i.e., at the vessel wall), for simplicity's we have the (constant) oxygen blood concentration $\sigma_b > \sigma_P$, although a more realistic flux condition might be imposed.

To determine the interface $r = \rho_N(t)$, we recall that the necrotic material cannot be converted back to living cells and that assumption (v) precludes having viable

cells when σ is smaller than σ_N. Thus the following inequalities must be satisfied:

$$u(\rho_N(t),t) - \dot{\rho}_N(t) \geq 0\,, \tag{8}$$

$$\sigma(\rho_N(t),t) \geq \sigma_N\,. \tag{9}$$

Therefore, from (8), two cases are possible: $u(\rho_N,t)-\dot{\rho}_N>0$ or $u(\rho_N,t)-\dot{\rho}_N=0$. If $u(\rho_N,t)-\dot{\rho}_N>0$ (i.e., if the cells cross the interface $\rho_N(t)$), the cord boundary is defined by the condition

$$\sigma(\rho_N(t),t) = \sigma_N\,, \tag{10}$$

and the interface is a "nonmaterial" free boundary. This case occurs, for instance, in the stationary state in the absence of treatment. Otherwise, the cord boundary becomes a "material" free boundary defined by

$$\dot{\rho}_N = u(\rho_N(t),t)\,. \tag{11}$$

The switch to the material interface may intervene when a sudden massive destruction of cells rapidly lowers oxygen consumption and the interface $\rho_N(t)$ defined by (10) tends to acquire a velocity larger than $u(\rho_N(t),t)$. The material boundary (11) is, however, subjected to the constraint (9) so that if $\sigma(\rho_N(t),t)$ tends to drop below σ_N during the cord repopulation, the free boundary must become nonmaterial again.

2.2. **Extracellular fluid motion and interstitial pressure.** It is assumed that (vi) the extracellular fluid flow is governed by the Darcy's law, consistently with the hypothesis that the cellular components of the cord form a porous structure (cf. [8]). The use of Darcy's law is widely accepted to describe the interstitial fluid flow (see [17]). According to this assumption, the velocity $\mathbf{v}$ of the extracellular fluid component is given by

$$(1-\nu^\star)(\mathbf{v}-\mathbf{u}) = -\kappa\nabla\hat{p}\,, \tag{12}$$

where $\hat{p}(r,z,t)$ is the fluid pressure and $\kappa>0$ is the hydraulic conductivity of the tissue. By summing (1)–(4), we obtain the overall incompressibility equation

$$\nabla\cdot(\mathbf{v}+\frac{\nu^\star}{1-\nu^\star}\mathbf{u}) = 0\,. \tag{13}$$

Instead of computing $\hat{p}(r,z,t)$, which satisfies an elliptic equation that can be derived by taking the divergence of equation (12) and using (13), we introduced an approximation that simplifies the problem of determining the longitudinal flow. Defining the longitudinal average

$$v(r,t) = \frac{1}{2H}\int_{-H}^{H} v_r(r,z,t)\,dz$$

and taking the longitudinal average of equation (13), we obtain

$$\frac{1}{r}\frac{\partial}{\partial r}(rv) + \frac{1}{2H}[v_z(r,H,t)-v_z(r,-H,t)] = -\frac{\nu^\star}{1-\nu^\star}\frac{1}{r}\frac{\partial}{\partial r}(ru)\,. \tag{14}$$

The volumetric efflux of liquid (per unit area) from the cord ends and at the radial distance r is approximated by

$$(1-\nu^\star)[v_z(r,H,t)-v_z(r,-H,t)] = 2\zeta_{out}(r)(p(r,t)-p_\infty)\,, \tag{15}$$

where $\zeta_{out}(r)$ is an assigned nonnegative function that represents the mean conductivity of the tissues traversed by the outgoing flux, p_∞ is a "far field" pressure identifiable with the pressure in the lymphatic vessels, and $p(r,t)$ is the longitudinal average of $\hat{p}$. Although the draining effect is likely to become active at a

certain distance from the blood vessel, we suppose here for simplicity $\zeta_{out}(r)=\zeta_{out}$ constant.

Having replaced the pressure with its longitudinal average, we obtain, from (14), (15), and (5), the following equation for the averaged radial velocity field $v(r,t)$:

$$\frac{1}{r}\frac{\partial}{\partial r}(rv) = -\frac{1}{1-\nu^\star}\left[\chi\nu_P-(1-\alpha)(\mu_P\nu_P+\mu_Q\nu_Q)-\mu_A(\nu^\star-\nu_P-\nu_Q)+\frac{\zeta_{out}}{H}(p-p_\infty)\right]. \tag{16}$$

At this point, the longitudinal average of the radial component of the Darcy equation (12),

$$(1-\nu^\star)(v-u) = -\kappa\frac{\partial p}{\partial r}\,,$$

yields the following equation for p:

$$p(r,t) = p_0(t) - \frac{1-\nu^\star}{\kappa}\int_{r_0}^{r}[v(r',t)-u(r',t)]\,dr'\,,$$

where $p_0(t)=p(r_0^+,t)$ is the pressure immediately outside the vessel wall; $p_0(t)$ is actually unknown, and the equation for p requires a condition at $r=\rho_N(t)$, which we will see in the next section. The equation (16) for v is complemented by the boundary condition at the vessel wall,

$$(1-\nu^\star)v(r_0,t) = \zeta_{in}(p_b-p_0(t))\,,$$

where ζ_{in} is the hydraulic conductivity of the wall and $p_b > p_\infty$ represents the longitudinal mean of the hydraulic pressure in the blood, corrected according to the jump of osmotic pressure.

2.3. **The necrotic region.** To model the necrotic region (N), in [6, 7] we assumed that an ideal arrangement of dead cells is maintained with a constant volume fraction equal to $\nu^\star$. This assumption is certainly questionable in view of the degradation process of dead cells and of the consequent loss of a coherent structure, and in [8] we took the very simplified and opposite view of representing N as a region completely filled with an incompressible viscous fluid having a uniform pressure. In this paper, still looking at the necrotic region as a compartment with uniform pressure, we take the more realistic approach of distinguishing the solid (cellular) from the liquid component, allowing the overall volume fraction of the cellular component to change. Since the necrotic cells retain some structural integrity before degradation [15], it appears reasonable that this fraction cannot exceed a maximal value less than the unity, corresponding to a close packing of cells. For simplicity, once again we take this limiting value equal to $\nu^\star$. Necrotic cells are assumed to be degraded to liquid with a rate constant μ_N.

In our geometry, the region N has the shape of a hollow cylinder with fixed bases $z=\pm H$ and moving lateral boundaries $r=\rho_N(t)$ and $r=B(t)$, both unknown. As previously stated, no flux takes place through the latter boundary. Let us denote by V_N^c the volume of the cellular component and by V_N^l the volume of the liquid component in N. Disregarding the loss of necrotic cells through the ends at $z=\pm H$, we can write the mass balance as

$$\dot V_N^c = 4H\pi\rho_N\nu^\star[u(\rho_N,t)-\dot\rho_N]-\mu_N V_N^c\,, \tag{17}$$

$$\dot V_N^l = 4H\pi\rho_N(1-\nu^\star)[v(\rho_N,t)-\dot\rho_N]+\mu_N V_N^c - q_{out}(t)\,, \tag{18}$$

where q_{out} is the volume efflux of liquid at $z=\pm H$. Similar to (15), we express q_{out} as follows:

$$q_{out} = 2\zeta_{out}^N \frac{V_N^l}{V_N^c + V_N^l} \pi (B^2 - \rho_N^2)(p_N - p_\infty)\,, \tag{19}$$

where ζ_{out}^N is a positive constant and p_N is the pressure in N. We will take $\zeta_{out}^N \geq \zeta_{out}/(1-\nu^\star)$, the strict inequality indicating a possibly facilitated efflux from the necrotic region. Since we exclude the formation of voids, the volume of the necrotic region, $V_N = 2H\pi(B^2-\rho_N^2)$, is equal to $V_N^c+V_N^l$. Then the total volume balance in N is expressed by

$$\dot{V}_N = 4H\pi\rho_N[(1-\nu^\star)v(\rho_N,t) + \nu^\star u(\rho_N,t) - \dot{\rho}_N] - \frac{\zeta_{out}^N}{H}(V_N - V_N^c)(p_N - p_\infty)$$

and the above equation can be rewritten as a differential equation for B^2,

$$\frac{dB^2}{dt} = 2\rho_N[(1-\nu^\star)v(\rho_N,t) + \nu^\star u(\rho_N,t)] - \frac{\zeta_{out}^N}{H}\big(B^2 - \rho_N^2 - \frac{V_N^c}{2H\pi}\big)(p_N - p_\infty)\,, \tag{20}$$

which has to be coupled to equation (17).

Let us point out that although (17) guarantees $V_N^c \geq 0$ because of (8), one cannot exclude that the limitation on the cellular fraction

$$\frac{V_N^c}{V_N^c + V_N^l} \leq \nu^\star \tag{21}$$

can be violated. Indeed, if too much liquid is removed or too much solid material is supplied, inequality (21) could be violated, which in our setting would be unphysical. Thus (21) has to be imposed as a constraint, the balance equations (17)–(18) keeping their validity. When (21) holds in the strict sense, we assume that the pressure p_N is determined by the displacement of the tissue that surrounds the whole tumor, whose size is likely to increase as B increases. Thus we write

$$p_N(t) = \Psi(B(t))\,, \tag{22}$$

where $\Psi(B)$ is an increasing function with $\Psi(B) \geq p_\infty$, and equations (17) and (20), together with (22), describe the evolution of B. On the contrary, when (21) takes the equality sign, V_N^l remains defined as

$$V_N^l = \frac{1-\nu^\star}{\nu^\star} V_N^c\,, \tag{23}$$

with V_N^c determined via equation (17), and the role of equation (18) is to provide $q_{out}(t)$. Hence $p_N(t)$ becomes a function of $B(t)$ no longer through (22) but through (23), (18), and (19). When the cellular fraction takes the limiting value $\nu^\star$, indeed, the action of the surroundings becomes supported by the cellular component, while the liquid pressure adjusts itself to preserve the volume balance, dropping necessarily below $\Psi(B)$ and reducing q_{out}. In this regime we have

$$p_N(t) = p_\infty + \frac{H}{\zeta_{out}^N}\left(\frac{2\rho_N[v(\rho_N,t) - u(\rho_N,t)]}{B^2 - \rho_N^2} + \frac{\mu_N}{1-\nu^\star}\right), \tag{24}$$

$$B(t) = \left(\rho_N^2 + \frac{V_N^c}{2H\pi\nu^\star}\right)^{1/2}. \tag{25}$$

Note that in this situation a stress on the solid component of the whole region $r_0 < r < B$ is created by the contact with the solid component of the neighboring cords at the boundary $r = B$. As a result, a stress is exerted on the central vessel,

which may have further consequences on the evolution of the tumor. For the sake of simplicity, we ignore this phenomenon and avoid the computation of the stresses.

During the evolution, equations (24) and (25) may lead in turn to a value of p_N that violates the constraint

$$p_N(t) \le \Psi(B(t))\,, \tag{26}$$

which is imposed by the deformation of the surrounding tissues. Then the system has to switch to the previous regime governed by (22) and (20), with V_N^l evolving according to (18) and constrained by (21). The switch has a clear physical explanation: the liquid component resumes the role of the stress supporting component in the necrotic region. To summarize, the evolution of the necrotic region takes place under a pair of unilateral contraints (i.e., the inequalities (21) and (26)), that decide which the correct governing equations are.

Assuming that the longitudinal average of the pressure is continuous across $r = \rho_N$, we will impose

$$p(\rho_N, t) = p_N(t)\,,$$

which gives the only missing information to determine the averaged pressure field in the cord.

3. **The model in nondimensional variables.** It is convenient to summarize the model equations, using the following nondimensional and normalized variables:

$$t' = t\chi\,, \qquad r' = \frac{r}{r_0}\,, \qquad z' = \frac{z}{H}\,,$$

$$u' = \frac{u}{\chi r_0}\,, \qquad v' = \frac{v}{\chi r_0}\,, \qquad p' = \frac{p - p_\infty}{p_b - p_\infty}\,, \qquad \sigma' = \frac{\sigma}{\sigma_b}\,,$$

$$\nu_P' = \frac{\nu_P}{\nu^\star}\,, \qquad \nu_Q' = \frac{\nu_Q}{\nu^\star}\,, \qquad \nu_A' = \frac{\nu_A}{\nu^\star}\,.$$

All the radial lengths, such as ρ_N and B, are rescaled by the radius r_0, and the volumes are rescaled by $r_0^2 H$; σ_b is used to rescale the thresholds on the oxygen concentration (σ_P, σ_Q, σ_N), and the transformation for p is used for $p_0\,, p_N$. All the rate costants, χ, γ, λ, μ_P, μ_Q, μ_A, μ_N, are rescaled by χ. For the other parameters and functions we have

$$\kappa' = \kappa \frac{p_b - p_\infty}{\chi r_0^2}\,, \qquad \zeta_{in}' = \zeta_{in} \frac{p_b - p_\infty}{\chi r_0}\,, \qquad \zeta_{out}' = \zeta_{out} \frac{p_b - p_\infty}{\chi H}\,,$$

$$\Psi'(B') = \frac{\Psi(B' r_0) - p_\infty}{p_b - p_\infty}\,, \qquad f_{P,Q}'(\sigma') = \frac{r_0^2}{\sigma_b} \nu^\star f_{P,Q}(\sigma' \sigma_b)\,.$$

For the sake of simplicity, the primes will be omitted in the following, and we will use the same symbol for the nondimensional and the dimensional quantity. The complete set of model equations is given below. Since, as it is easy to check, if (5) holds, any solution of equations (1)–(3) will have a sum equal to $\nu^\star$ provided that the initial conditions satisfy this property, the equation for ν_A will be omitted. For $r \in (1, \rho_N)$, we have

$$\frac{\partial \nu_P}{\partial t} + u \frac{\partial \nu_P}{\partial r} = \nu_P \big[(1 - \nu_P) + (1 - \alpha)(\mu_P \nu_P + \mu_Q \nu_Q) + \mu_A (1 - \nu_P - \nu_Q) - \lambda(\sigma) - \mu_P\big] + \gamma(\sigma) \nu_Q\,, \tag{27}$$

$$\frac{\partial \nu_Q}{\partial t} + u \frac{\partial \nu_Q}{\partial r} = \nu_Q \big[-\nu_P + (1 - \alpha)(\mu_P \nu_P + \mu_Q \nu_Q) + \mu_A (1 - \nu_P - \nu_Q) - \gamma(\sigma) - \mu_Q\big] + \lambda(\sigma) \nu_P\,, \tag{28}$$

$$\frac{1}{r}\frac{\partial}{\partial r}(ru) = \nu_P - (1-\alpha)(\mu_P\nu_P + \mu_Q\nu_Q) - \mu_A(1-\nu_P-\nu_Q)\,, \tag{29}$$

$$\Delta\sigma = f_P(\sigma)\nu_P + f_Q(\sigma)\nu_Q\,, \tag{30}$$

$$\frac{1}{r}\frac{\partial}{\partial r}(rv) = -\frac{\nu^\star}{1-\nu^\star}\left[\nu_P - (1-\alpha)(\mu_P\nu_P+\mu_Q\nu_Q) - \mu_A(1-\nu_P-\nu_Q) + \frac{1}{\nu^\star}\zeta_{out}\,p\right],$$

$$p(r,t) = p_0(t) - \frac{1-\nu^\star}{\kappa}\int_1^r [v(r',t)-u(r',t)]\,dr'\,,$$

$$p(\rho_N,t) = p_N(t)\,,$$

$$\frac{dV_N^c}{dt} = 4\pi\rho_N\nu^\star[u(\rho_N,t)-\dot\rho_N] - \mu_N V_N^c\,. \tag{31}$$

Moreover, either

$$p_N(t) = \Psi(B(t))\,,$$

$$\frac{dB^2}{dt} = 2\rho_N[(1-\nu^\star)v(\rho_N,t) + \nu^\star u(\rho_N,t)] - \zeta_{out}^N\big(B^2-\rho_N^2-\frac{V_N^c}{2\pi}\big)\Psi(B)\,, \tag{32}$$

under the condition

$$\frac{V_N^c}{2\pi(B^2-\rho_N^2)} < \nu^\star\,,$$

or

$$p_N(t) = \frac{1}{\zeta_{out}^N}\left(\frac{2\rho_N[v(\rho_N,t)-u(\rho_N,t)]}{B^2-\rho_N^2} + \frac{\mu_N}{1-\nu^\star}\right),$$

$$B(t) = \left(\rho_N^2 + \frac{V_N^c}{2\pi\nu^\star}\right)^{1/2},$$

under the condition

$$p_N(t) \le \Psi(B(t))\,.$$

The boundary and interface conditions for σ and v are those given in section 2, suitably transformed by recalling that in the nondimensional setting $r_0=1$, $\sigma_b=1$, $p_b=1$, and $p_\infty=0$. The results that follow are given in terms of the nondimensional variables and parameters.

4. **The steady state.** In the absence of treatment ($\mu_P=\mu_Q=0$), the only cell populations present in the cord at the stationary state are the viable proliferating and quiescent subpopulations, and $\nu_P+\nu_Q=1$. Thus, from (27)–(29) we obtain for ν_P the equation

$$u\frac{\partial\nu_P}{\partial r} = \nu_P(1-\nu_P) - \lambda(\sigma)\nu_P + \gamma(\sigma)(1-\nu_P)\,, \quad 1<r<\rho_N\,, \tag{33}$$

where $u(r)$ is given by

$$ru(r) = \int_1^r r'\nu_P(r')\,dr'\,. \tag{34}$$

Equations (33) and (34) must be solved together with equation (30), with the boundary conditions (6), (7), and (10), to obtain the time-independent solution $\nu_P(r)$, $u(r)$, $\sigma(r)$ and the constant cord radius ρ_N (Problem A). The existence and uniqueness of this stationary solution has been proved in [8] under a slight restriction on λ and γ. Note that equation (33) is degenerate at $r=r_0$ because $u(r_0)=0$. However, according to our assumptions on the shape of $\lambda(\sigma)$ and $\gamma(\sigma)$, there will exist an inner region of the cord (where $\sigma>\sigma_P$) in which these transition rates are constant. Thus, the solution ν_P is constant for $1<r<\rho_P$, with the radius ρ_P such that $\sigma(\rho_P)=\sigma_P$. Moreover, it can be proved that the volume fraction ν_P is decreasing with r and remains positive in the interval $(\rho_P,\rho_N]$, even if $\gamma_{min}=0$.

The numerical solution of Problem A was computed according to a procedure that suitably modifies the one described in [6]. In all the simulations presented here, the functions f_P and f_Q are assumed equal, and $f_P(\sigma)$ has the form

$$f_P(\sigma) = F\frac{\sigma}{K+\sigma}\,,$$

which we derived from [9].

Once Problem A is solved, V_N^c can be computed as $4\pi\rho_N\nu^\star u(\rho_N)/\mu_N$, and we can obtain the functions $v(r)$, $p(r)$ in $[1,\rho_N]$ and the constants p_0, p_N, and B, satisfying the constraints (21) and (26) and the equations (Problem B)

$$\frac{1}{r}\frac{\partial}{\partial r}(rv) = -\frac{1}{1-\nu^\star}\big(\nu^\star\nu_P + \zeta_{out}\,p\big)\,, \tag{35}$$

$$v(1) = \frac{1}{1-\nu^\star}\zeta_{in}(1-p_0)\,, \tag{36}$$

$$p(r) = p_0 - \frac{1-\nu^\star}{\kappa}\int_1^r [v(r') - u(r')]\,dr'\,, \tag{37}$$

$$p(\rho_N) = p_N\,,$$

and either

$$p_N = \Psi(B)\,,$$

$$\zeta_{out}^N\big(B^2 - \rho_N^2 - 2\rho_N\frac{u(\rho_N)\nu^\star}{\mu_N}\big)\Psi(B) = 2\rho_N[(1-\nu^\star)v(\rho_N) + \nu^\star u(\rho_N)] \tag{38}$$

or

$$p_N = \frac{1}{\zeta_{out}^N}\big[\frac{2\rho_N[v(\rho_N)-u(\rho_N)]}{B^2-\rho_N^2} + \frac{\mu_N}{1-\nu^\star}\big]\,, \tag{39}$$

$$B = B^\star = \big[\rho_N^2 + 2\rho_N\frac{u(\rho_N)}{\mu_N}\big]^{1/2}.$$

Equation (38) is obtained from equations (31) and (32) written at the stationary state. Note that if the constraint (21) is satisfied in the strict sense, B will be larger than $B^\star$. In [8] the existence and uniqueness of the solution of Problem B was proved in the limit case of an immediate degradation of dead cells entering N, that is, in the case of $\mu_N \to \infty$.

The numerical solution of Problem B is based on the fact that the solution of equations (35)–(37) depends univocally on p_0. This fact suggested the following fixed-point iterative procedure. Let p_0^k denote the value of p_0 at the step k. We go through the following procedure:

- Given p_0^k, we solve the integro-differential equation for v obtained by substituting (37) into (35), with the initial condition (36), using the implicit Euler method.
- We find B^k by solving equation (38) for B through the bisection method and compute $p_N^k = \Psi(B^k)$.
- From (37) written for $r = \rho_N$, setting $p(\rho_N) = p_N^k$ we compute $p_0 = \bar{p}_0^k$.
- We update p_0 by means of

$$p_0^{k+1} = \varepsilon\bar{p}_0^k + (1-\varepsilon)p_0^k\,. \tag{40}$$

In (40), the parameter $\varepsilon \leq 1$ is suitably chosen to guarantee convergence. Next the condition (21) is checked, and if it is not satisfied, the procedure is repeated setting $B^k = B^\star$ and computing p_N^k through equation (39). For the function $\Psi(B)$ we have chosen the expression

$$\Psi(B) = e(B-1)^2$$

to approximate the nonlinear elasticity of biological tissues, with e being a given elasticity coefficient.

In the numerical simulations, the adimensional parameter values were chosen with reference to the following baseline values of the dimensional parameters that, whenever possible, have been selected according to available experimental data: $r_0 = 20\,\mu$m [16], $H = 300\,\mu$m, $\nu^\star = 0.85$, $\chi = \ln 2/24\,\mathrm{h}^{-1}$, $p_b = 20$ mmHg, $p_\infty = 0$ mmHg, $\sigma_b = 40$ mmHg, $F = 1.51 \cdot 10^{-2}$ mmHg/μm^2 [9], $K = 4.32$ mmHg [9], $\zeta_{in} = 10.08\,\mu\mathrm{m}\cdot\mathrm{mmHg}^{-1}\cdot\mathrm{h}^{-1}$ [4], and κ in the range $2.63{\cdot}10^3 \div 86.4{\cdot}10^3\,\mu\mathrm{m}^2\cdot\mathrm{mmHg}^{-1}\cdot\mathrm{h}^{-1}$ [17].

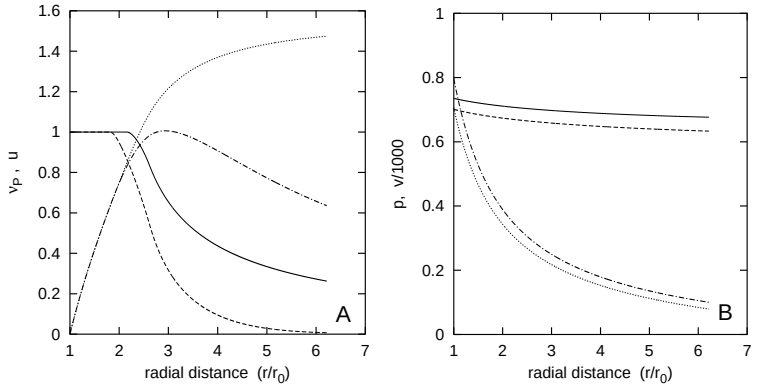

FIGURE 2. Panel A, profiles of $\nu_P(r)$ and $u(r)$: for pair 1 ($\lambda_{max} = 1$ and $\sigma_P = 0.375$), ν_P is solid line and u is dotted line; for pair 2 ($\lambda_{max} = 2$ and $\sigma_P = 0.5$), ν_P is dashed line and u is dashed-dotted line. Panel B, profiles of $p(r)$ and $v(r)$: for pair 1, p is solid line and v is dotted line; for pair 2, p is dashed line and v is dashed-dotted line. Other parameters: $\sigma_Q = 0.25$, $\sigma_N = 0.0125$, $F = 0.128$, $K = 0.108$, $\gamma_{max} = 4$, $\lambda_{min} = \gamma_{min} = 0$, $\nu^\star = 0.85$, $\zeta_{in} = 400$, $\zeta_{out} = 2$, $\kappa = 3000$, $e = 12 \cdot 10^{-3}$, $\zeta_{out}^N = \zeta_{out}/(1-\nu^\star)$, and $\mu_N = 1$.

Figure 2A shows the profiles of $\nu_P(r)$ and $u(r)$ for two different pairs λ_{max} and σ_P, assuming $\lambda_{min} = \gamma_{min} = 0$. Since $\lambda_{min} = 0$, $\nu_P(r) = 1$ until r is less than ρ_P, and then ν_P decreases, the larger slope corresponding to the larger value of λ_{max}. In the case of $\lambda_{max} = 2$ and $\sigma_P = 0.5$, the percentage of proliferating cells in the cord is reduced (0.210 vs. 0.487), and consequently the cell velocity u is also lower. The corresponding profiles of $p(r)$ and $v(r)$ are shown in Figure 2B. The pressure p_0 is a substantial fraction of p_b, and $p(r)$ exhibits a slight decrease with r, thus retrieving the experimental observation of a large interstitial pressure. The slope of p depends on the Darcy coefficient: the assumed value of κ is in the typical range of tumor tissues [17]. The fluid velocity v is very high with respect to the cell velocity u. When the fraction of proliferating cells is larger and $u(\rho_N)$ is increased, the model predicts an increase of B. The actual increment is small (8.51 vs. 8.26),

because the relatively high value of the rate constant μ_N causes the presence of a large amount of liquid in the necrotic region ($V_N^c/V_N = 0.46$). As a consequence of the increase of B, a limited increase of pressure in the necrotic region is predicted, together with an increase in the whole profile $p(r)$. Thus the influx of fluid from the central vessel is decreased, reducing the velocity v.

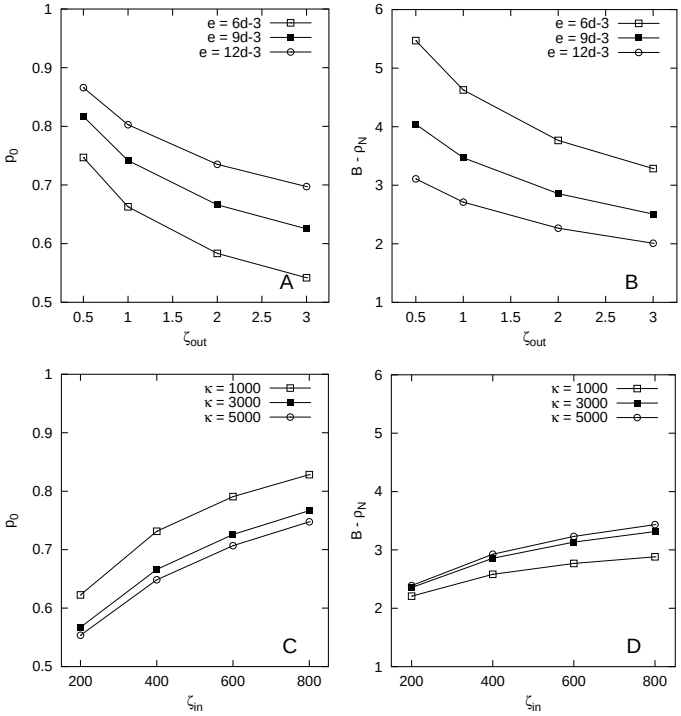

FIGURE 3. Panels A and B: p_0 and B as a function of ζ_{out} for different values of e. Panels C and D: p_0 and B as a function of ζ_{in} for different values of κ, with $e = 9 \cdot 10^{-3}$. Other parameters are as in Figure 2, with $\lambda_{max} = 1$ and $\sigma_P = 0.375$.

Since we do not have experimental data on the values of the parameters ζ_{out} and e, and because ζ_{in} and κ may present large variations in different tumors, we have explored numerically the effect of changes in these parameters. Figure 3 reports the predicted changes of p_0 (taken as representative of interstitial pressure) and of B. As expected, when ζ_{out} increases (facilitating the outflow from the cord) B and p_0 decrease. However, when the stiffness of the surrounding tissue is higher, an increased interstitial pressure may be accompanied by a diminished radius of the necrotic region because p_N may be increased (panels A and B). Panels C and D show instead that as ζ_{in} increases, both B and p_0 increase. A reduced κ produces an increase in p_0, because a steeper gradient of p is established. A higher value of p_0 counteracts the advantage of a higher ζ_{in} in producing a higher influx from the vessel, so for low κ values, the increase in B with ζ_{in} is smaller.

The effect of parameter changes on the mean fluid velocity is illustrated in Figure 4. As expected, the mean fluid velocity increases as ζ_{in} increases, but this increase is markedly modulated by changes in the other parameters. When ζ_{out} increases,

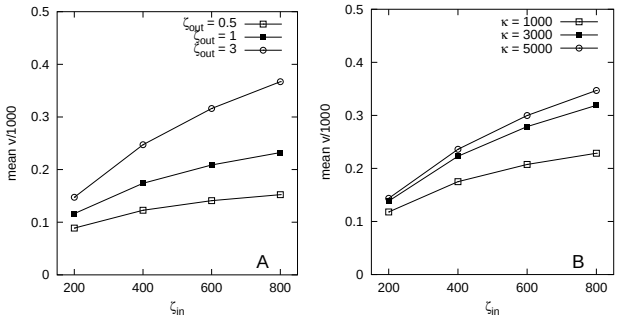

FIGURE 4. Mean value of the fluid velocity as a function of ζ_{in} for different values of ζ_{out} (panel A) and κ (panel B), with $e = 9 \cdot 10^{-3}$. Other parameters are as in Figure 2, with $\lambda_{max} = 1$ and $\sigma_P = 0.375$.

two competing effects can occur: the radial component of fluid velocity decreases to a greater extent because of the facilitated efflux from the cord ends, and the initial fluid velocity $v(1)$ increases because p_0 decreases (see Fig. 3A). The resulting effect is in general an increase of the mean v as shown by Figure 4A. The increase in mean v with ζ_{in} appears to be enhanced as κ increases (Fig. 4B), since, as seen in Figure 3C, higher κ values give lower p values and then a greater $v(1)$.

In all the above numerical simulations, note that the constraint (21) was never violated, although it is not difficult to find instances in which the opposite is true, with parameter values still chosen in a reasonable range.

5. **Change of interstitial pressure and fluid velocity after cell killing.** Let us now consider the changes of the interstitial pressure and of the extracellular fluid velocity following the delivery of a cell-killing agent. We will assume the stationary state described in section 4 as the initial condition. We restrict ourselves to considering a single-dose treatment, and we choose for $\mu_P(r,t)$ and $\mu_Q(r,t)$ the following space-independent expressions:

$$\mu_P(r,t) = \frac{m_P}{\tau_1 - \tau_2}(\mathrm{e}^{-t/\tau_1} - \mathrm{e}^{-t/\tau_2}),$$
$$\mu_Q(r,t) = \frac{m_Q}{\tau_1 - \tau_2}(\mathrm{e}^{-t/\tau_1} - \mathrm{e}^{-t/\tau_2}),$$

where m_P, m_Q, τ_1 and τ_2 are parameters suitably chosen to mimic the effect of a drug delivered as a single bolus. As in the steady-state problem, the time evolution of ν_P, ν_Q, u, σ, ρ_N, and V_N^c (Problem A) is independent of the time evolution of p, v, and B (Problem B).

The numerical solution of Problem A is based on a procedure that suitably extends that described in [6]. The basic feature of this procedure is the computation of the viable cell fractions along a prefixed set of characteristic lines of equations (27)–(28). The numerical computation of p, v, and B was performed in parallel, guaranteeing that the constraints (21) and (26) are satisfied.

Figure 5 reports an example of the time evolution of the cord for different values of ζ_{out}. The radius ρ_N shows an initial shrinkage, followed by a regrowth that will eventually lead the cord to the stationary state (panel A). The interface ρ_N quickly becomes a material boundary and so remains until, after $t = 4$, it becomes nonmaterial again. This event is marked by a slope discontinuity. In the same

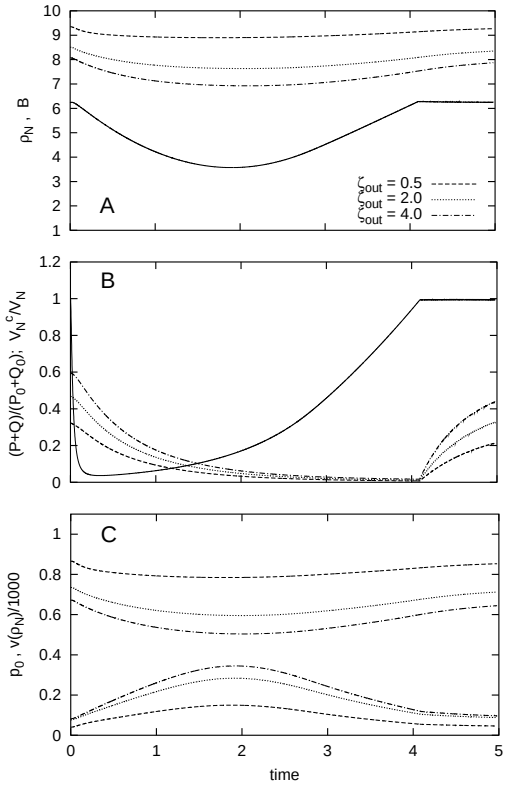

FIGURE 5. Panel A: time course of ρ_N (solid line) and of B (dashed curves). Panel B: ratio between the volume of total viable cells, $P+Q$, at time t, and its value at $t=0$ (solid line); cellular fraction in N (dashed curves). Panel C: time course of p_0 (upper curves) and of $v(\rho_N)$ (lower curves). The values of ζ_{out} are as indicated, with $m_P = m_Q = 4$, $\tau_1 = 0.087$, $\tau_2 = \tau_1/20$, $\alpha = 0.7$, and $\mu_A = 1$. Other parameters are as in Figure 2, with $\lambda_{max} = 1$ and $\sigma_P = 0.375$.

panel, the time course of the boundary B is plotted. Boundary B has a slighter regression, as compared with that of ρ_N, because the necrotic region tends to be filled by liquid. As expected, this regression is smaller for smaller values of ζ_{out}. Panel B reports the ratio between the total volume (per unit cord length) of viable cells and its value at $t = 0$, showing the dynamics of the viable-cell population following the treatment (the drug bolus reduces the viable cells to around 1/20 of the initial value), together with the cellular fraction in the necrotic region. This fraction decays until the interface ρ_N is material, because the cellular volume V_N^c, according to equation (31), is no longer fed by the dead cells. When the interface ρ_N returns to nonmaterial, V_N^c is fed again. Panel C shows that the pressure p_0 (upper curves) diminishes after the treatment, basically because of the decrease of B (and then of p_N). The decrease of p_0 causes an increase of the fluid velocity out of the vessel wall, $v(1)$, and this increment contributes to the observed increment in $v(\rho_N)$ (lower curves). This fact suggests that after a first dose of drug, there is a time interval in which the convective extravasation of the drug is facilitated. The increase in $v(1)$ related to the decrease of p_0, together with the net production of

liquid due to the disgregation of dead cells within the cord, may explain the very moderate regression of the necrotic region.

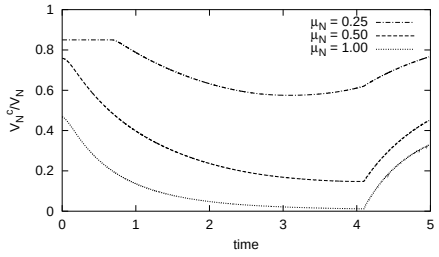

FIGURE 6. Time course of the cellular fraction in N for different values of μ_N. Other parameters are as in Figure 5, with $\zeta_{out}=2$.

In the cases of Figure 5B, the necrotic region rapidly becomes almost completely composed by liquid. This phenomenon is however modulated by the degradation rate of necrotic cells, and as may be seen in Figure 6, the cellular fraction can be enhanced as μ_N is lowered. For the smallest value of μ_N ($\mu_N=0.25$), the constraint (21) is active with the equality sign until $t=0.68$. After this time, B and p_N switch to the regime defined by equations (20) and (22), and the cellular fraction in N goes below $\nu^\star$. As the cord regrows to the steady state, at $t=5.93$ (not shown in the figure), the system switches again to the regime characterized by a cellular fraction equal to $\nu^\star$.

6. **Concluding remarks.** The model illustrated here describes, in the ideal geometry of a regular array of parallel tumor cords, the interstitial pressure and the extracellular fluid motion in terms of longitudinal averages of the pressure and of the radial component of the fluid velocity, respectively. The model recovers the experimentally observed high value of the interstitial pressure, postulating a relatively low value of the parameters ζ_{out} and ζ_{out}^N, which summarize the high hydraulic resistance that fluid encounters when flowing into lymphatic vessels. Our investigation focusses on the case in which necrosis is present in the tumor mass. The model assigns a role to the necrotic region in determining the interstitial pressure in the viable region, as it may sense the forces produced by the displacement of the surrounding tissue during tumor growth. In the presence of high interstitial pressure, a limited convective current is predicted, indicating a possibly reduced transport of anticancer agents with high molecular weight. After a single-dose cell-killing treatment, the model predicts a very limited regression of the necrotic region, due to a substantial filling of this region by liquids. This finding suggests that the overall regression of the tumor mass after treatments may be explained only by taking into account variations in time of the parameters that characterize the balance of fluid. In particular, phenomena such as the impairment of the vascular network and the enhancement of the hydraulic conductivities, due to cell death and degradation of dead cells, should be accounted for.

Acknowledgment. This work was partially supported by the FIRB-MIUR project "Metodi dell'Analisi Matematica in Biologia, Medicina e Ambiente."

REFERENCES

[1] Ø. Åmellem and E. O. Pettersen, Cell-cycle progression in human-cells following re-oxygenation after extreme hypoxia—consequences concerning initiation of DNA-synthesis, Cell Prolif. 26 (1993) 25–35.

[2] R. P. Araujo and D. L. S. McElwain, A history of the study of solid tumour growth: the contribution of mathematical modelling, Bull. Math. Biol. 66 (2004) 1039–1091.

[3] J. W. Baish, P. A. Netti, and R. K. Jain, Transmural coupling of fluid flow in micro-circulatory network and interstitium in tumors, Microvasc. Res. 53 (1997) 128–141.

[4] L. T. Baxter and R. K. Jain, Transport of fluid and macromolecules in tumors. I. Role of interstitial pressure and convection, Microvasc. Res. 37 (1989) 77–104.

[5] N. Bellomo, E. De Angelis, and L. Preziosi, Multiscale modeling and mathematical problems related to tumor evolution and medical therapy, J. Theor. Med. 5 (2003) 111–136.

[6] A. Bertuzzi, A. d'Onofrio, A. Fasano, and A. Gandolfi, Regression and regrowth of tumour cords following single-dose anticancer treatment, Bull. Math. Biol. 65 (2003) 903–931.

[7] A. Bertuzzi, A. Fasano, and A. Gandolfi, A free boundary problem with unilateral constraints describing the evolution of a tumour cord under the influence of cell killing agents, SIAM J. Math. Anal. 36 (2004) 882–915.

[8] A. Bertuzzi, A. Fasano, and A. Gandolfi, A mathematical model for tumour cords incorporating the flow of interstitial fluid, Math. Mod. Meth. Appl. Sci. (to appear).

[9] J. J. Casciari, S. V. Sotirchos, and R. M. Sutherland, Variations in tumor cell growth rates and metabolism with oxygen concentration, glucose concentration, and extracellular pH, J. Cell. Physiol. 151 (1992) 386–394.

[10] M. A. J. Chaplain, From mutation to metastasis: The mathematical modelling of the stages of tumour development, in A Survey of Models for Tumor-Immune System Dynamics, eds. J. A. Adam and N. Bellomo, Birkhäuser, Boston, 1997, 187–236.

[11] A. Friedman, A hierarchy of cancer models and their mathematical challenges, Discrete Contin. Dynam. Systems B 4 (2004) 147–159.

[12] D. G. Hirst and J. Denekamp, Tumour cell proliferation in relation to the vasculature, Cell Tissue Kinet. 12 (1979) 31–42.

[13] R. K. Jain, Delivery of molecular medicine to solid tumors: Lessons from in vivo imaging of gene expression and function, J. Controlled Release 74 (2001) 7–25.

[14] A. Krogh, The number and distribution of capillaries in muscles with calculations of the oxygen pressure head necessary for supplying the tissue, J. Physiol. 52 (1919) 409–415.

[15] G. Majno and I. Joris, Apoptosis, oncosis and necrosis: An overview of cell death, Am. J. Pathol. 146 (1995) 3–15.

[16] J. V. Moore, P. S. Hasleton, and C. H. Buckley, Tumour cords in 52 human bronchial and cervical squamous cell carcinomas: Inferences for their cellular kinetics and radiobiology, Br. J. Cancer 51 (1985) 407–413.

[17] P. A. Netti and R. K. Jain, Interstitial transport in solid tumours, in Cancer Modelling and Simulation, ed. L. Preziosi, Chapman and Hall/CRC, Boca Raton, FL, 2003, 51–74.

[18] J. A. Royds, S. K. Dower, E. E. Qwarnstrom, and C. E. Lewis, Response of tumour cells to hypoxia: Role of p53 and NFκB, J. Clin. Pathol. Mol. Pathol. 51 (1998), 55–61.

[19] I. F. Tannock, The relation between cell proliferation and the vascular system in a transplanted mouse mammary tumour, Br. J. Cancer 22 (1968) 258–273.

[20] W. L. Walker and J. Cook, Drug delivery to brain tumors, Bull. Math. Biol. 58 (1996) 1047–1074.

Received on January 1, 2005. Revised on June 8, 2005.

E-mail address: bertuzzi@iasi.cnr.it
E-mail address: fasano@math.unifi.it
E-mail address: gandolfi@iasi.cnr.it
E-mail address: sinisgalli@iasi.cnr.it